Available online at website: https://journal.bcrec.id/index.php/bcrec

Bulletin of Chemical Reaction Engineering & Catalysis, 19 (2) 2024, 340-349

Research Article

# Synthesis and Characterisation of Graphene Oxide Catalysts for Glycerol Acetylation

**Nur Hidayati[1,*], Wahib Khoiruddin[1], Herry Purnama[1], Marwan Effendy[2]**

[1]*Department of Chemical Engineering, Universitas Muhammadiyah Surakarta, Jalan Ahmad Yani No. 157, Pabelan, Kartasura, Sukoharjo, 57169, Indonesia.*
[2]*Department of Mechanical Engineering, Universitas Muhammadiyah Surakarta, Jalan Ahmad Yani No. 157, Pabelan, Kartasura, Sukoharjo, 57169, Indonesia.*

*Received: 22nd April 2024; Revised: 15th June 2024; Accepted: 15th June 2024*
*Available online: 8th July 2024; Published regularly: August 2024*

## Abstract

Glycerol in large quantities as a by-product of biodiesel production is a promising feedstock to be converted into more valuable products such as acetin. In this work, acetin converted from glycerol acetylation with acetic acid was performed over graphene oxide as a catalyst in a batch reactor. The study's objective was to evaluate the effect of sodium nitrate amount in the catalyst preparation on the catalyst's characteristics and catalytic performance. The graphene oxide (GO) catalysts were characterised by various tests, such as SEM-EDX for their morphology, the nitrogen adsorption capacity using Breneur-Emmet Teller (BET), structural analysis using XRD, functional group using FTIR, and catalytic activity on glycerol acetylation. The GO1, GO2, and GO3 catalysts were varied based on the $NaNO_3$ amount in the modified Hummer method. The experiments found that the $NaNO_3$ amount in catalyst preparation plays a vital role in GO structure formation. The GO2 catalyst has the highest performance, as indicated by the highest surface area, pore volume, and size. High glycerol conversion (94 %) and selectivity toward the interest products of triacetin (24 %) and diacetin + triacetin (83 %) were reached in 2 h of reaction using three wt.% catalysts, 110 °C reaction temperature, and 1:9 molar ratio of glycerol to acetic acid.



***Keywords***: Acetylation; Catalytic Activity; Glycerol; Graphene Oxide; MWCNTs

***How to Cite***: N. Hidayati, W. Khoiruddin, H. Purnama, M. Effendy (2024). Synthesis and Characterisation of Graphene Oxide Catalysts for Glycerol Acetylation. *Bulletin of Chemical Reaction Engineering & Catalysis*, 19 (2), 340-349 (doi: 10.9767/bcrec.20146)

***Permalink/DOI***: https://doi.org/10.9767/bcrec.20146

## 1. Introduction

Petroleum-based commodities provide almost 85% of the world's energy [1]. Air pollution, harmful exhaust pollutants, and greenhouse gas emissions increase with conventional fuel use [2]. Energy from biomass is more sustainable and environmentally favorable than fossil fuels [3]. Using biomass to generate biofuels like methanol, ethanol, bio-crude, biodiesel, and methane to replace fossil fuels is popular. Renewable and environmentally friendly, biodiesel is a popular green energy source [4]. Biodiesel's biodegradability, lower greenhouse gas emissions than gasoline fuels, equivalent energy durability, renewability, and low carbon monoxide and sulphur dioxide emissions are its key benefits [5–8]. Transesterification of triglycerides and low-molecular-weight alcohols with an alkaline catalyst creates biodiesel. Triglyceride feed sources include vegetable, animal fat, waste cooking oil, microbial and algal oils [9–11], and fatty acids from the catalytic cracking of triglycerides [12]. A study found that global biodiesel output is rising, adding 10% glycerol [13].

The conversion of glycerol into value-added products is necessary to support the long-term growth of the chemical industry. By acetylating glycerol with acetic acid or acetic anhydride, glycerol could be transformed into mono-, di-, and tri-acetin [14,15]. The diverse industrial

* Corresponding Author.
Email: nur.hidayati@ums.ac.id (N. Hidayati)

applications of these acetate ester products range from cryogenics and cosmetics to effective fuel additives [15] that improve fuel viscosity and act as an anti-knock agent for biodiesel and increase the octane number of gasoline. The selectivity of this glycerol product is dependent on the catalyst employed.

Acetylation of glycerol to acetin could be accomplished using either homogeneous or heterogeneous catalysts. Commonly used homogeneous catalysts include HCl, $H_2SO_4$, $H_3PO_4$, and ionic acid solutions such N-methyl-2-pyrrolidinium hydrogen sulfate [16,17]. Because they are corrosive, homogeneous catalysts cause disposal problems. It is preferable to use heterogeneous catalysts because they are less harmful to the environment and make it easier to separate the reaction products from the catalyst itself. The main challenge of catalytic glycerol acetylation is the low selectivity of di- and tri-acetin [18,19], and some solid catalysts are not commercially applicable in the industry [15]. The use of enzyme catalysts is very stable. It could be used for as many as 15 cycles, does not have an effect of corrosion on the reactor, and could be easily separated from the medium in which the reaction is taking place [20]. However, the use of enzyme catalysts still has some drawbacks, the most notable of which is a long reaction time, which can last up to twenty-four hours. As a result, the amount of energy that must be consumed is significant, and the enzyme is quickly rendered inactive due to the impurities present in glycerol. Amberlyst-35 [21], Amberlyst-15 [22], [23], zirconia [24,25], heteropolyacid based [26] and niobic acid [27], and zeolite [28,29] are some of the heterogeneous acid catalysts that have been developed. Carbon-based solid acid catalysts offer good catalysis in the esterification of methanol with acetic acid due to their high stability, activity, and selectivity [30] and demonstrate promising glycerol acetylation activity and selectivity [31].

According to research by Khayoon and Hameed, sulfonated activated carbon possesses stable catalytic activity and a high degree of selectivity regarding glycerol acetylation reactions [32]. Graphene oxide (GO), which is made from graphite, has been shown to be a useful catalyst for acetylating alcohols and phenols, with high yields in a short reaction time and mild conditions [33]. GO has also attracted attention as a catalyst for biodiesel synthesis due to its unique characteristics [34]. To the best of our knowledge, there has yet to be an investigation into the utilisation of GO as a catalyst for the acetylation of glycerol. Previously, we reported the performance of GO prepared using the modified Hummer method for optimising glycerol acetylation [35]. GO could be created using the Hummers method and its modifications. The classic Hummers method uses sulphuric acid as a mixture of oxidising compounds, while the modified Hummers uses sulphuric acid and sodium nitrate [36]. It is estimated that the amount of sodium nitrate as an oxidising compound in the MWCNT oxidation process affects the characteristics of the resulting GO. This study focuses on evaluating the graphene oxide made of MWCNT as a catalyst for acetylation of glycerol to acetin, examining the amount of nitrate on the MWCNT oxidation process the physicochemical characteristics of graphene oxide catalysts, and its activity on the acetylation reaction of glycerol to acetin.

## 2. Materials and Methods

Three graphene oxide (GO) catalysts were developed using Hummer's method modification by varying $NaNO_3$ in sulphuric acid as an oxidising compound in the MWCNT oxidation. The catalyst characterisation was realised using SEM-EDX**,** Breneur-Emmet Teller (BET), X-ray diffraction (XRD), and Fourier Transform Infrared (FTIR) Spectroscopy. All catalysts also were performed on glycerol acetylation.

### 2.1 Materials

The material used in the experiments was multi-walled carbon nanotubes (MWCNT) from Jiangsu XFNANO Materials China. The ingredients were sulphuric acid (98%) and hydrochloric acid (37%) from Mallinckrodt, potassium permanganate from VWR Life Science, phosphoric acid (85%), sodium nitrate (>99.5%), glycerol (85 %), acetic acid (>99.5%), chloroform (99.4%), periodic acid (99%), hydrogen peroxide (50%), potassium iodide (99.5%), sodium thiosulfate (99%), potassium dichromate (99.9%) from Merck, and ethanol (99.5%) from Ajax Finechem.

### 2.2 Catalyst Preparation

The process of catalyst preparation was carried out using a modified Hummer method. A total of 3 g of MWCNT powder was dissolved in 69 mL 98 % $H_2SO_4$ and 0.5, 1.0, or 1.5 g of $NaNO_3$ according to the ratio to be tested. One hour was then spent stirring the mixture. The temperature was maintained between 0 and 20 °C for 4 h, while 8 g of $KMnO_4$ was added gradually to the mixture while stirring. The mixture turned into greenish-black colour. The stirring process was continued for 20 h at 35 °C. The mixture then turned light brown in colour. The mixture was then washed with 200 mL of distilled water and stirred for 1 h. The mixture was added with 20 mL of 30 % $H_2O_2$ to remove the remaining $KMnO_4$. Subsequently, the mixture was washed with 80 mL of HCl and

distilled water repeatedly to neutralise the pH. When the pH became neutral, the solid material was dried at 110 °C for 12 h to obtain a GO catalyst. Furthermore, the catalysts were named GO1, GO2, and GO3 according to the amount of $NaNO_3$.

2.3 GO Catalyst Characteristics

The morphological characteristics and elemental composition of MWCNT and GO catalyst were evaluated using images acquired using a JEOL JSM 7500F scanning electron microscope equipped with an energy dispersive X-ray analyser which operated at 10-20 kV. The Breneur-Emmet Teller (BET) test was carried out to ascertain the surface characteristics, such as the surface area ($m^2/g$), pore diameter (nm), and pore volume ($cm^3/g$). An isotherm was determined for the absorption and desorption of nitrogen gas on the surface at a temperature of 77 K. The information was acquired through the use of Quantachrome TouchWin version 1.11.

An XRD test was carried out to ascertain the crystal structure and crystal size of a solid material. An X'Pert Pro diffractometer from PANalytical type PW 3040/60 was used to measure the X-ray diffraction pattern using Cu-Kα radiation at 0.154 nm, 30 mA, and 40 kV. Samples were observed continuously at 2θ around 5 – 90°. Identification of the sample phase utilised Match v.1.1. An FTIR analysis was conducted to identify the functional groups responsible for forming bonds with the catalyst. Perkin Elmer Spectrum IR Software Version 10.6.1 was utilised to record the spectrum at vibrations ranging from 400 to 4000 $cm^{-1}$.

2.4 GO Catalyst Activity Test

The acetylation reaction of glycerol with acetic acid was carried out in a three-neck flask that was fitted with a condenser. This flask was used to carry out the GO catalyst activity. Glycerol with a volume of 19.13 mL and a GO catalyst of 3 % glycerol mass was put into a three-neck flask and heated to a reaction temperature of 110 ºC and with a magnetic stirrer speed of 800 rpm. The acetic acid that had been preheated to a temperature of 100 ºC was put into a three-neck flask with a ratio of glycerol: acetic acid = 1:9. The temperature was maintained at a steady 110 °C throughout. Every 15 min, a sample was taken to determine the remaining unreacted glycerol in mass percentage, using iodometric titration and calculated by Equation (1) [37,38]. The standard approach entails the oxidation of glycerol and the subsequent measurement of the resulting released iodine, which is subsequently titrated using sodium thiosulfate. The glycerol conversion and acetin selectivity are calculated respectively using equations (2) and (3), where $B$ is volume of $Na_2S_2O_3$ solution in blank titration (mL), $S$ is volume of $Na_2S_2O_3$ solution in sample titration (mL), $N$ is normality of $Na_2S_2O_3$ solution, $W$ is sample weight (g).

$$Glycerol\ content\ (\%m) = \frac{2{,}302(B-S)N}{W} \quad (1)$$

$$X(\%) = \frac{the\ reacting\ glycerol\ mass}{the\ initial\ glycerol\ mass} \times 100\% \quad (2)$$

$$S(\%) = \frac{mass\ of\ produced\ mono\ or\ di\ or\ triacetin}{the\ reacting\ glycerol\ mass} \times 100\% \quad (3)$$

The reaction product solution was tested using GCMS (Shimadzu QP2010 SE, Rtx-5MS column (30 m, 0.25 mm, 0.25 μm) to determine the composition of acetin.

## 3. Results and Discussion

The synthesis and characterisation of graphene oxide catalysts for glycerol acetylation

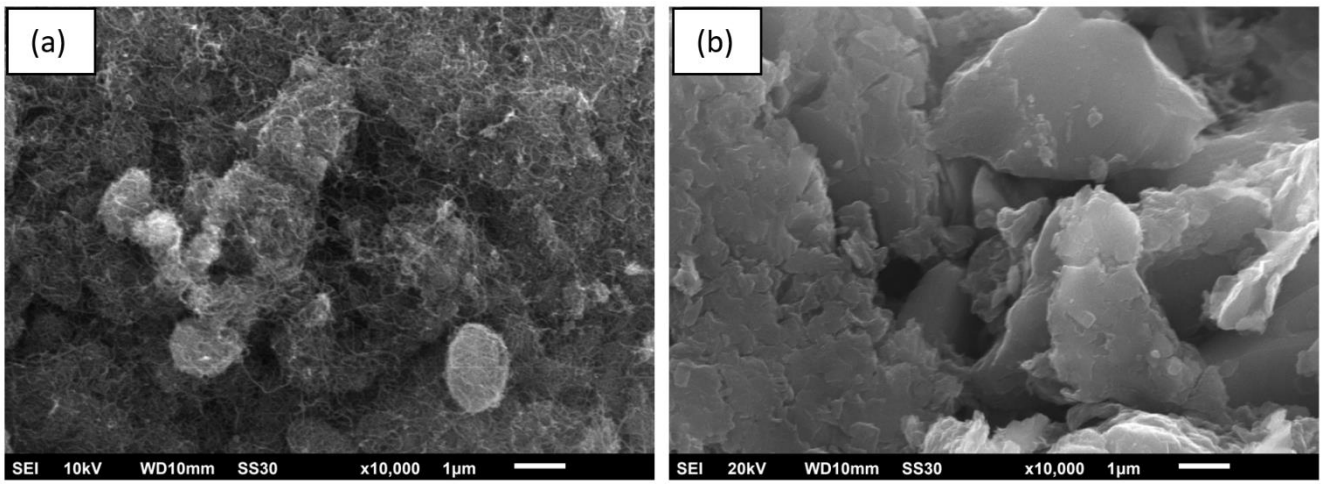


Figure 1. The SEM images of (a) MWCNT and (b) GO2.

have been studied experimentally. The morphology analysis with SEM-EDX, analysis of the surface area, volume, and pore size with BET, structural analysis with XRD, functional group analysis with FTIR, and catalytic activity on glycerol acetylation was used to characterise three variants of graphene oxide (GO) catalysts. The following are the main findings and the advanced discussion.

3.1 SEM-EDX

The SEM images of the untreated MWCNT and selected sample of GO2 particles at a magnification of 10000x are presented in Figure 1, and the elemental composition is listed in Table 1. The tubular structure of untreated MWCNT is depicted in Figure 1(a), while the image of the GO2 catalyst is shown in Figure 1(b). The GO2 catalyst has a flake-like structure with wrinkled surfaces, which can be attributed to the formation of oxygen-containing functional groups and Sp3 carbons in the basal planes [39] and indicates a high oxidation level [40]. When oxygen-containing groups are introduced, MWCNT can expand significantly perpendicular to the carbon layer plane, increasing the thickness of the resulting GO nanosheets; as seen in the SEM image, GO2 looks thicker than MWCNT.

The oxygen content of the GO2 catalyst is significantly higher than that of the MWCNT. The atomic C:O ratio identifies the degree of oxidation. Because of the presence of oxygen-containing functional groups on the edge and basal planes, a highly oxidised MWCNT has a low atomic C:O ratio [41]. The elemental composition of the GO2 catalyst is presented in Table 1, revealing that the C:O ratio is dramatically lower (2.4:1) than that of MWCNT (33.1:1).

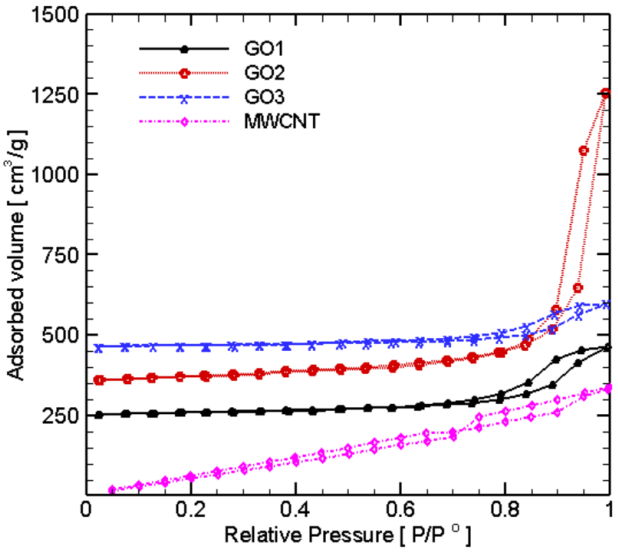


Figure 2. The adsorption-desorption of $N_2$ isotherm on GO and MWCNT.

3.2 BET Analysis

The specific surface area was determined using BET analysis and multilayer nitrogen adsorption, which was measured as a function of relative pressure and covered the outer area of the solid as well as the area of the pores. Barret-Joyner-Halenda (BJH) analysis was used to determine the pore area and specific pore volume using adsorption and desorption techniques. This technique was also used to characterise the pore size distribution. Table 2 displays the BET surface area, volume, and pore size measurements for GO and MWCNT catalysts. Figure 2 depicts the profile of the $N_2$ gas isotherm adsorption-desorption catalyst tested.

During the process of treating the carbon, the porous structure of the oxidised carbon is created. It is possible to close pores by isolating them from one another. Alternatively, pores can be connected

Table 1. The elemental composition of MWCNT and GO2.

| Elements | MWCNT | | GO2 | |
|---|---|---|---|---|
| | Mass % | Atom % | Mass % | Atom % |
| C | 96.14 | 97.07 | 64.02 | 70.01 |
| O | 3.85 | 2.93 | 35.60 | 29.25 |
| S | 0.00 | 0.00 | 0.35 | 0.14 |

Table 2. Diffraction peaks and d-spacing MWCNT and GO catalysts at 2θ (002) and (100) planes.

| Catalysts | (002) | | (100) | |
|---|---|---|---|---|
| | 2θ | d-spacing (Å) | 2θ | d-spacing (Å) |
| MWCNT | 25.84 | 3.445 | 43.96 | 2.058 |
| GO1 | 25.81 | 3.450 | 43.58 | 2.075 |
| GO2 | 25.44 | 3.498 | 43.96 | 2.058 |
| GO3 | 25.74 | 3.458 | 43.48 | 2.079 |

so that their sizes and shapes are the same or different [42]. The resultant GO catalyst increases the pore size from 3.9 nm for MWCNT to about 8 – 13 nm, while the pore volumes of GO1 and GO3 decrease compared to MWCNT, but GO2 increases. According to the dominance of pore size in the range of 3.9 – 18 nm, the IUPAC classifies it as a solid with a mesoporous structure [42]. According to the IUPAC classification and as demonstrated in Figure 2, all of the catalyst samples (MWCNT and GO) show a type IV isotherm with a hysteresis loop for GO H1 and MWCNT H3. Monolayer-multilayer adsorption by porous materials with well-defined cylinder-like pore channels or agglomerates of uniform planes is associated with the H1 hysteresis loop. While the hysteresis circle H3 is related to slit-shaped pores, as shown by the fact that its pore size is smaller than that of the GO catalyst, the GO catalyst has larger pores.

Generally, the surface area decreased dramatically from the initial material MWCNT (457.01 $m^2/g$) to graphene oxide (varying from 64 to 186.68 $m^2/g$). The change in the surface area of the catalyst is significantly influenced by the mole ratio of sulphuric acid to sodium nitrate used in the reaction. Both sulphuric acid and sodium nitrate play the role of solvents, making it possible for protonated carbon to be oxidised by $KMnO_4$ in straightforwardly [43]. Equation 4 describes the reaction between sulphuric acid and sodium nitrate.

$$2NaNO_3 + H_2SO_4 \rightarrow 2HNO_3 + Na_2SO_4 \quad (4)$$

The nitric acid produced by this reaction acts as an oxidising agent. The mole ratio of sulphuric acid to sodium nitrate determines the amount of nitric acid produced, which influences the strength of the carbon protonation. The protonation of carbon bonds that are too strong can lead to the collapse of the pore walls, leading to agglomeration and a reduction in the pore volume. This was demonstrated by the fact that GO3 has a relatively low pore volume and surface area. Carbon Nano Tubes (CNTs) that had been covalently bonded with functionalised sulphonic acid polymer compounds were found by Liu *et al.* to have experienced a significant reduction in both their surface area and pore volume [44]. However, the protonation strength of the oxidizing agent alone does not solely determine the surface area of GO. The overall strength of the oxidation process and the exact conditions under which it occurs are also vital factors. The amount of exfoliation, the interlayer spacing, and the introduction and density of functional groups all affect these parameters, which taken together define the accessible surface area of GO.

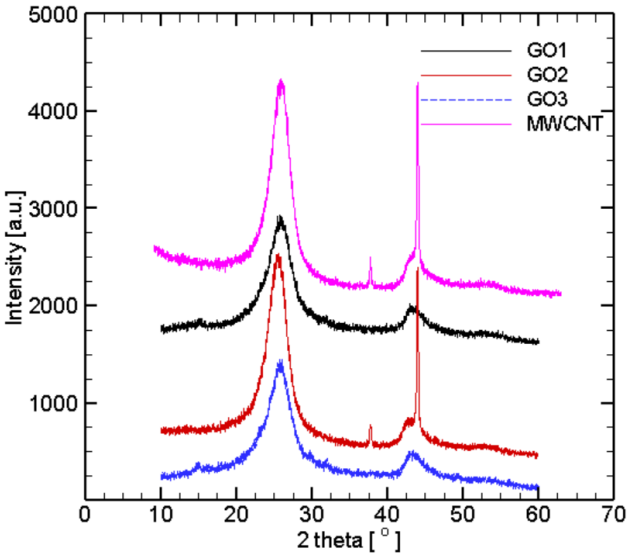


Figure 3. XRD diffractogram graph of MWCNT and GO.

### 3.3 XRD Analysis

MWCNT and GO catalyst microstructure was investigated through XRD in a series of experiments. Figure 3 shows the XRD diffraction patterns of both the MWCNT and GO catalysts. The diffraction pattern identifies two distinct peaks of carbon at values of 2θ around 25 and 43, which correspond to the crystallographic planes (002) and (100), respectively [44]. According to the diffraction pattern, the 2θ value of (002) MWCNT peak shifts to the left from 25.84° to 25.81°, 25.44° and 25.74° at GO1, GO2, and GO3, respectively. Diffraction shifts to the left, and d-spacing increases (Table 3) due to the unzipping and exfoliation of MWCNT. The widening and shifting of the diffraction peaks (002) are what determine the percentage of successful GO formation that results from MWCNT exfoliation [45]. Almost the same pattern occurs at the peak of the

Table 3. The catalyst texture.

| Property | Catalyst | | | |
|---|---|---|---|---|
| | MWCNT | GO1 | GO2 | GO3 |
| Pore Volume ($cm^3/g$) | 0.529 | 0.346 | 1.425 | 0.220 |
| Pore Size (nm) | 3.900 | 8.020 | 13.060 | 8.040 |
| BET Surface Area ($m^2/g$) | 457.01 | 104.86 | 186.68 | 64.00 |

crystallographic plane (100). The amorphous carbon in GO1 and GO3, which consists of randomly oriented polycyclic aromatic carbon sheets, is associated with a decrease in diffraction intensity at 2θ around 25 in those two compounds [46]. The absence of the characteristic peak around 11° 2θ in XRD patterns of GO samples may be attributed to the lower level of oxidation, which affects the structure of GO. The high diffraction intensity at two around 43 in MWCNT and GO2 indicates a high content of crystalline carbon. In contrast, the low crystalline carbon content in GO1 and GO3 is indicated by the fact that GO1 and GO3 contain less of it. Moreover, the crystallite sizes of MWCNT and GO2 are around 3-13 nm, while those of GO1 and GO3 are less than 5 nm, which are calculated using the Scherrer equation.

### 3.4 FTIR Analysis

The Fourier transform infrared spectroscopy (FTIR) was utilised to identify compounds and detect functional groups in a sample. The FTIR spectrum of MWCNT and GO catalyst at wave numbers 400 – 4000 $cm^{-1}$ is depicted in Figure 4. GO has a hexagonal carbon structure, but it also includes such as hydroxyl groups (−OH), epoxy (C−O−C), carbonyl (C=O), and carboxylic acids (−COOH) [47]. The hydroxyl group can be easily identified on the catalyst GO, which is represented by the band that can be found between 3000 $cm^{-1}$ and 3800 $cm^{-1}$ [48]. The presence of carboxylic groups (−COOH) in GO can be identified based on multiple peaks that can be found at wave numbers between 1700 and 1750 $cm^{-1}$ for C=O stretching vibration, at wave number 1400-1440 $cm^{-1}$ for O−H bending vibration, and at wave number around 1200-1300 $cm^{-1}$ for C−O strecthing vibration. In GO, the intensity of the vibration of the C=C group at around 1575-1625 $cm^{-1}$ is found to be greater than in MWCNT. A higher degree of oxidation in the basal plane of graphene due to the isolation of more aromatic rings is indicated by an increase in the vibration intensity of the C=C bond [49]. The peak at 1100-1300 $cm^{-1}$ in the vibration extension mode indicates the presence of C−O stretching vibration as corrreponding epoxy and carboxyl group.

### 3.5 Catalyst Performance on Glycerol Acetylation

Acetylation of glycerol into acetin using GO catalyst was carried out at a temperature of 110 °C, and the amount of catalyst was 3% of the reacted glycerol mass. The performance of GO catalysts on the acetylation reaction can be seen in Figure 5. In general, the glycerol conversion increases by increasing the reaction time. The highest performance is shown by the GO2 catalyst, which during the reaction time of 120 min, achieves up to 94% glycerol conversion. The GO2 performance may have something to do with the character of the surface area, volume and pore size of the GO2 catalyst, which is the highest among other catalysts. The large surface area of the catalyst allows the reactants to be well adsorbed, thereby increasing the reaction rate. The XRD testing also supports GO2's performance against glycerol acetylation reaction. The GO2 catalyst indicates that the value of 2θ from the crystallisation plane (002) shifts to the far left compared to other catalysts. This indicates intercalation in the tube (intratube) between sulfate and nitrate ions with better coaxial graphene cylinders. The FTIR test confirms these

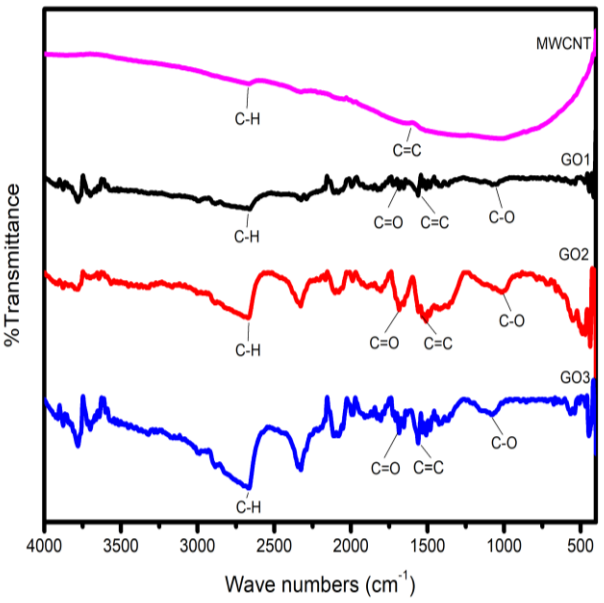


Figure 4. FTIR spectrum of MWCNT and GO.

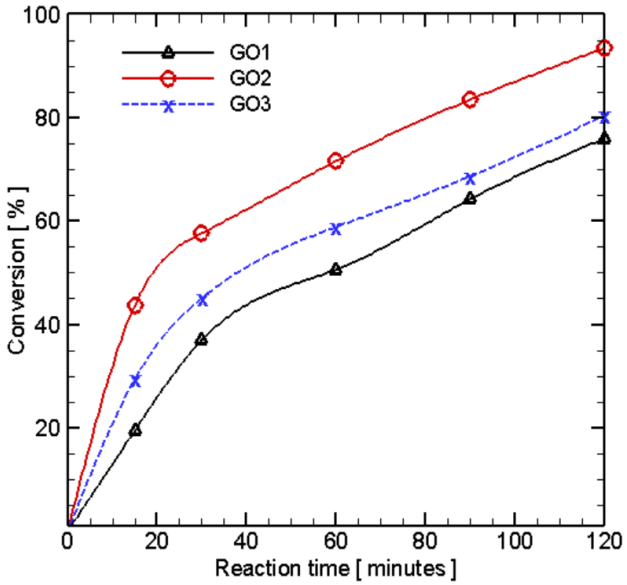


Figure 5. Glycerol conversion as a function of time and type of catalyst.

results, where the presence of a carbonyl group (C=O) shows a higher vibration intensity than the GO1 and GO3 catalysts, which represents the success of MWCNT oxidation. The carbonyl group bounded in this GO might have a vital role in the mechanism of the glycerol acetylation reaction.

A test using GCMS was carried out to identify the composition of acetin. Figure 6 shows the chromatogram of the reaction products, and Table 4 reports the components and composition of acetin. The figure shows seven dominant peaks representing acetin. The first and fourth peaks of the chromatogram are for monoacetin, the second and fifth peaks are for diacetin, and the sixth and seventh peaks are for triacetin. The GCMS analysis proves diacetin dominates at approximately 57 % and 26 % for triacetin.

The performance of GO catalysts can be compared with the performance of other carbon catalysts (Table 5), with some even showing better performance. Some carbon catalysts are reported to require a longer time, higher temperature, and higher amount of catalyst but the conversion value and selectivity of triacetin obtained were similar. However, further testing is needed to improve the performance of this GO catalyst.

## 4. Conclusion

Multi-walled carbon nanotubes (MWCNT) have been successfully synthesised as a carbon source into graphene oxide (GO) using the modified Hummers method. It could be summarised that the ratio of sulphuric acid and sodium nitrate as a solution facilitated the protonation of MWCNT when the oxidation process using $KMnO_4$ affected the crystal structure of GO. The presence of a carbonyl group that might be required during the catalysis

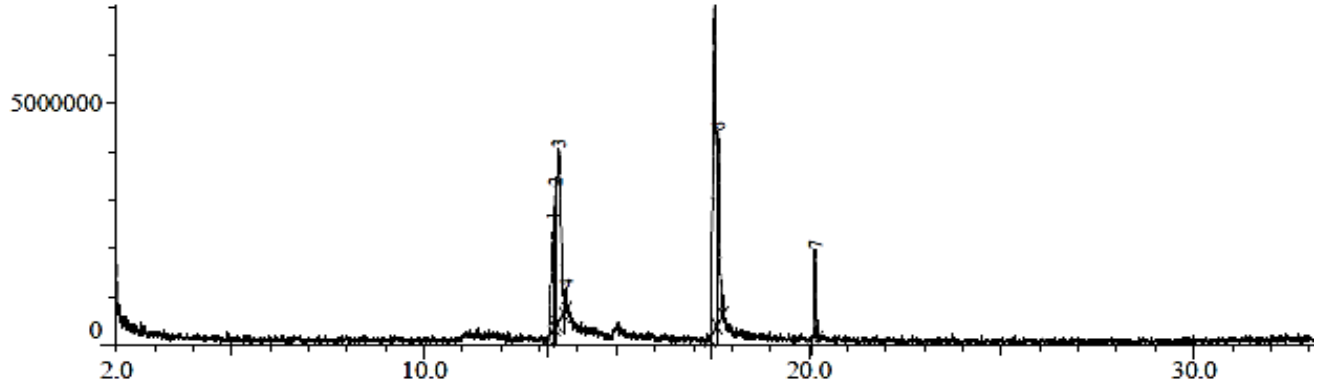


Figure 6. The GC-MS chromatogram of GO2 catalyzed reaction products.

Table 4. Selectivity of glycerol into mono, di and triacetin.

| Acetin Compound | Molecular weight (g/mol) | Peak | Selectivity (%) | |
|---|---|---|---|---|
| Mono- | 134 | 1<br>4 | 14.87<br>1.72 | 16.60 |
| Di- | 176 | 2<br>5 | 13.00<br>44.15 | 57.15 |
| Tri- | 218 | 6<br>7 | 20.08<br>6.17 | 26.25 |
| TOTAL | | | 100 | 100 |

Table 5. The comparison of glycerol acetylation catalyst performance.

| Catalyst | Reaction Condition | | | | *X* (%) | *S* (%) | Ref. |
|---|---|---|---|---|---|---|---|
| | *T* (°C) | Mole Ratio | % catalyst | *t* (min) | | | |
| Carbon from biomass | 120 | 1:6 | 10 | 180 | 99 | 22-35 | [46] |
| Cr base metal organic/ activated C | 110 | 1:9 | 4 | 300 | 100 | 5.2 | [50] |
| UiO-66/activated C | 90 | 1:6 | 5 | 180 | n.a. | 17.9 | [51] |
| Y2O3/ Palm Kernel Shell derived C | 130 | 1:12 | 10 | 300 | 99.8 | 29.6 | [52] |
| Plastic waste derived C | 110 | 1:6 | 9 | 60 | 95 | 20 | [53] |
| Graphene Oxide | 110 | 1:9 | 3 | 120 | 94 | 26 | This Work |

process occurred. Glycerol conversion reached about 94 % during the 2-hour reaction time. Thus the GO catalyst is feasible to be developed as a solid catalyst for the glycerol acetylation reaction to produce acetin.

**Acknowledgements**

The authors gratefully acknowledge the financial support from the Ministry of Research and Technology / National Agency for Research and Innovation Indonesia through the National Competitive Basic Research Fund via Universitas Muhammadiyah Surakarta under contract number 199.17/A.3-LPPM/V/2019. The first author would also like to thank Nia Murniawati and Ravina Nabila for characterising the catalysts.

**CRedit Authors Statement**

Nur Hidayati: Conceptualization, Methodology, Investigation, Writing, Review and Editing, Validation, Supervision, Funding acquisition; Wahib Khoiruddin: Resource, Investigation, Original Draft, Formal Analysis, Data Curation, Project Administration; Herry Purnama: Validation, Writing, Review and Editing; Marwan Effendy: Software, Writing, Review and Editing, Visualization. All authors have read and agreed to the published version of the manuscript.

**References**

[1] Azarpour, A., Mohammadzadeh, O., Rezaei, N., Zendehboudi, S. (2022). Current status and future prospects of renewable and sustainable energy in North America: Progress and challenges. *Energy Conversion and Management*, 269, 115945. DOI: 10.1016/j.enconman.2022.115945.

[2] Balikowa, A., Effendy, M., Ngafwan, N., Wandera, C. (2023). The impacts of nanoscale silica particle additives on fuel atomisation and droplet size in the internal combustion engines: A review. *Applied Research and Smart Technology (ARSTech)*, 4(2), 92–111. DOI: 10.23917/arstech.v4i2.2759.

[3] Ong, H.C., Chen, W.-H., Farooq, A., Gan, Y.Y., Lee, K.T., Ashokkumar, V. (2019). Catalytic thermochemical conversion of biomass for biofuel production: A comprehensive review. *Renewable and Sustainable Energy Reviews*, 113, 109266. DOI: 10.1016/j.rser.2019.109266.

[4] Sahani, S., Roy, T., Chandra Sharma, Y. (2019). Clean and efficient production of biodiesel using barium cerate as a heterogeneous catalyst for the biodiesel production; kinetics and thermodynamic study. *Journal of Cleaner Production*, 237, 117699. DOI: 10.1016/j.jclepro.2019.117699.

[5] Caldas, B.S., Nunes, C.S., Souza, P.R., Rosa, F.A., Visentainer, J. V., Júnior, O. de O.S., Muniz, E.C. (2016). Supercritical ethanolysis for biodiesel production from edible oil waste using ionic liquid [HMim][HSO4] as catalyst. *Applied Catalysis B: Environmental*, 181, 289–297. DOI: 10.1016/j.apcatb.2015.07.047.

[6] Gardy, J., Hassanpour, A., Lai, X., Ahmed, M.H., Rehan, M. (2017). Biodiesel production from used cooking oil using a novel surface functionalised TiO2 nano-catalyst. *Applied Catalysis B: Environmental*, 207, 297–310. DOI: 10.1016/j.apcatb.2017.01.080.

[7] Singh, V., Belova, L., Singh, B., Sharma, Y.C. (2018). Biodiesel production using a novel heterogeneous catalyst, magnesium zirconate (Mg2Zr5O12): Process optimization through response surface methodology (RSM). *Energy Conversion and Management*, 174, 198–207. DOI: 10.1016/j.enconman.2018.08.029.

[8] Rajak, U., Verma, T.N. (2018). Effect of emission from ethylic biodiesel of edible and non-edible vegetable oil, animal fats, waste oil and alcohol in CI engine. *Energy Conversion and Management*, 166, 704–718. DOI: 10.1016/j.enconman.2018.04.070.

[9] Purnama, H., Harland, Hidayati, N. (2020). Biodiesel from microalgae Nannochloropsis oculata and Tetraselmis chuii by sonication technique and $K_2CO_3$ catalyst. *IOP Conference Series: Materials Science and Engineering*, 821(1), 012011. DOI: 10.1088/1757-899X/821/1/012011.

[10] Banković-Ilić, I.B., Stamenković, O.S., Veljković, V.B. (2012). Biodiesel production from non-edible plant oils. *Renewable and Sustainable Energy Reviews*, 16(6), 3621–3647. DOI: 10.1016/j.rser.2012.03.002.

[11] Bizualem, Y.D., Nurie, A.G. (2024). A review on recent biodiesel intensification process through cavitation and microwave reactors: Yield, energy, and economic analysis. *Heliyon*, 10(2), e24643. DOI: 10.1016/j.heliyon.2024.e24643.

[12] Musthofa, M., Lee, J., Harvey, A. (2015). Catalytic Cracking of Triglyceride Over Sulphated Zirconia Solid Catalyst: Process, Kinetics, and Mechanism. In: Olabi, A.G., Alaswad, A. (eds). Paisley: Proceeding of SEEP, pp. 11–14.

[13] Khayoon, M.S., Hameed, B.H. (2011). Acetylation of glycerol to biofuel additives over sulfated activated carbon catalyst. *Bioresource Technology*, 102(19), 9229–9235. DOI: 10.1016/j.biortech.2011.07.035.

[14] Liao, X., Zhu, Y., Wang, S.G., Li, Y. (2009). Producing triacetylglycerol with glycerol by two steps: Esterification and acetylation. *Fuel Processing Technology*, 90(7–8), 988–993. DOI: 10.1016/j.fuproc.2009.03.015.

[15] Khayoon, M.S., Hameed, B.H. (2011). Acetylation of glycerol to biofuel additives over sulfated activated carbon catalyst. *Bioresource Technology*, 102(19), 9229–9235. DOI: 10.1016/j.biortech.2011.07.035.

[16] Okoye, P.U., Hameed, B.H. (2016). Review on recent progress in catalytic carboxylation and acetylation of glycerol as a byproduct of biodiesel production. *Renewable and Sustainable Energy Reviews*, 53, 558–574. DOI: 10.1016/j.rser.2015.08.064.

[17] Keogh, J., Tiwari, M.S., Manyar, H. (2019). Esterification of Glycerol with Acetic Acid Using Nitrogen-Based Brønsted-Acidic Ionic Liquids. *Industrial & Engineering Chemistry Research*, 58, 17235–17243. DOI: 10.1021/acs.iecr.9b01223.

[18] Kong, P.S., Aroua, M.K., Daud, W.M.A.W., Lee, H.V., Cognet, P., Pérès, Y. (2016). Catalytic role of solid acid catalysts in glycerol acetylation for the production of bio-additives: A review. *RSC Advances*, 6(73), 68885–68905. DOI: 10.1039/c6ra10686b.

[19] Sun, J., Tong, X., Yu, L., Wan, J. (2016). An efficient and sustainable production of triacetin from the acetylation of glycerol using magnetic solid acid catalysts under mild conditions. *Catalysis Today*, 264, 115–122. DOI: 10.1016/j.cattod.2015.07.011.

[20] Tudorache, M., Negoi, A., Protesescu, L., Parvulescu, V.I. (2014). Biocatalytic alternative for bio-glycerol conversion with alkyl carbonates via a lipase-linked magnetic nano-particles assisted process. *Applied Catalysis B: Environmental*, 145, 120–125. DOI: 10.1016/j.apcatb.2012.12.033.

[21] Liao, X., Zhu, Y., Wang, S.G., Chen, H., Li, Y. (2010). Theoretical elucidation of acetylating glycerol with acetic acid and acetic anhydride. *Applied Catalysis B: Environmental*, 94, 64–70. DOI: 10.1016/j.apcatb.2009.10.021.

[22] Gonçalves, V.L.C., Pinto, B.P., Silva, J.C., Mota, C.J.A. (2008). Acetylation of glycerol catalyzed by different solid acids. *Catalysis Today*, 133–135(1–4), 673–677. DOI: 10.1016/j.cattod.2007.12.037.

[23] Caballero, K.V., Guerrero-Amaya, H., Baldovino-Medrano, V.G. (2019). Revisiting glycerol esterification with acetic acid over Amberlyst-35 via statistically designed experiments: Overcoming transport limitations. *Chemical Engineering Science*, 207, 91–104. DOI: 10.1016/j.ces.2019.06.003.

[24] Reddy, P.S., Sudarsanam, P., Raju, G., Reddy, B.M. (2010). Synthesis of bio-additives: Acetylation of glycerol over zirconia-based solid acid catalysts. *Catalysis Communications*, 11(15), 1224–1228. DOI: 10.1016/j.catcom.2010.07.006.

[25] Chamack, M., Mahjoub, A.R., Akbari, A. (2018). Zirconium-modified mesoporous silica as an efficient catalyst for the production of fuel additives from glycerol. *Catalysis Communications*, 110, 1–4. DOI: 10.1016/j.catcom.2018.02.021.

[26] Veluturla, S., Narula, A., D, S.R., Shetty, S.P. (2017). Kinetic study of synthesis of bio-fuel additives from glycerol using a hetropolyacid. *Resource-Efficient Technologies*, 3, 337–341. DOI: 10.1016/j.reffit.2017.02.005.

[27] Balaraju, M., Nikhitha, P., Jagadeeswaraiah, K., Srilatha, K., Sai Prasad, P.S., Lingaiah, N. (2010). Acetylation of glycerol to synthesize bioadditives over niobic acid supported tungstophosphoric acid catalysts. *Fuel Processing Technology*, 91(2), 249–253. DOI: 10.1016/j.fuproc.2009.10.005.

[28] Kowalska-Kus, J., Held, A., Nowinska, K. (2016). Enhancement of the catalytic activity of H-ZSM-5 zeolites for glycerol acetalization by mechanical grinding. *Reaction Kinetics, Mechanisms and Catalysis*, 117(1), 341–352. DOI: 10.1007/s11144-015-0922-4.

[29] Jyoti Konwar, L., Mäki-arvela, P., Begum, P., Kumar, N., Jyoti, A., Mikkola, J., Chandra, R., Deka, D. (2015). Shape selectivity and acidity effects in glycerol acetylation with acetic anhydride : Selective synthesis of triacetin over Y-zeolite and sulfonated mesoporous carbons. *Journal of Catalysis*, 329, 237–247. DOI: 10.1016/j.jcat.2015.05.021.

[30] Gupta, P., Paul, S. (2014). Solid acids: Green alternatives for acid catalysis. *Catalysis Today*, 236(PART B), 153–170. DOI: 10.1016/j.cattod.2014.04.010.

[31] Hidayati, N., Sari, R.P., Purnama, H. (2020). Catalysis of glycerol acetylation on solid acid catalyst: a review. *Jurnal Kimia Sains dan Aplikasi*, 23(12), 414–423. DOI: 10.14710/jksa.23.12.414-423.

[32] Khayoon, M.S., Hameed, B.H. (2011). Acetylation of glycerol to biofuel additives over sulfated activated carbon catalyst. *Bioresource Technology*, 102(19), 9229–9235. DOI: 10.1016/j.biortech.2011.07.035.

[33] Liu, Y.-Y., Qi, J.-M., Bai, L.-S., Xu, Y.-L., Ma, N., Sun, F.-F. (2016). Graphite oxide-catalyzed acetylation of alcohols and phenols. *Chinese Chemical Letters*, 27(5), 726–730. DOI: 10.1016/j.cclet.2016.01.005.

[34] Mushahary, N., Sarkar, A., Basumatary, F., Brahma, S., Das, B., Basumatary, S. (2024). Recent developments on graphene oxide and its composite materials: From fundamentals to applications in biodiesel synthesis, adsorption, photocatalysis, supercapacitors, sensors and antimicrobial activity. *Results in Surfaces and Interfaces*, 15, 100225. DOI: 10.1016/j.rsurfi.2024.100225.

[35] Hidayati, N., Maulida, I.R., Purnama, H., Musthofa, M., Ur Rahmah, A. (2024). Optimisation of the glycerol acetylation process using graphene oxide catalyst. *South African Journal of Chemical Engineering*, 48, 254–264. DOI: 10.1016/j.sajce.2024.02.005.

[36] Chang, C., Chang, K., Shen, H., Hu, C. (2014). A unique two-step Hummers method for fabricating low-defect graphene oxide nanoribbons through exfoliating multiwalled carbon nanotubes. *Journal of the Taiwan Institute of Chemical Engineers*, 45(5), 2762–2769. DOI: 10.1016/j.jtice.2014.05.030.

[37] Setyaningsih, L., Siddiq, F., Pramezy, A. (2018). Esterification of glycerol with acetic acid over Lewatit catalyst. *MATEC Web of Conferences*, 154, 2–5. DOI: 10.1051/matecconf/201815401028.

[38] Badan Standardisasi Nasional (2015). *Biodiesel SNI 7182, 2015*.

[39] Al-Gaashani, R., Najjar, A., Zakaria, Y., Mansoura, S., Atieh, M.A. (2019). XPS and structural studies of high quality graphene oxide and reduced graphene oxide prepared by different chemical oxidation methods. *Ceramics International*, 45(11), 14439–14448. DOI: 10.1016/j.ceramint.2019.04.165.

[40] Alkhouzaam, A., Qiblawey, H., Khraisheh, M., Atieh, M., Al-Ghouti, M. (2020). Synthesis of graphene oxides particle of high oxidation degree using a modified Hummers method. *Ceramics International*, 46(15), 23997–24007. DOI: 10.1016/j.ceramint.2020.06.177.

[41] Higginbotham, A.L., Kosynkin, D. V, Sinitskii, A., Sun, Z., Tour, J.M. (2010). Lower-Defect Graphene Oxide Nanotubes. *ACS nano*, 4(4), 2059. DOI: 10.1021/nn100118m.

[42] Alothman, Z.A. (2012). A Review: Fundamental Aspects of Silicate Mesoporous Materials. *Materials*, 5(12), 2874-2902 DOI: 10.3390/ma5122874

[43] Smith, A.T., Marie, A., Zeng, S., Liu, B., Sun, L. (2019). Nano Materials Science Synthesis, properties, and applications of graphene oxide / reduced graphene oxide and their nanocomposites. *Nano Materials Science*, 1(1), 31–47. DOI: 10.1016/j.nanoms.2019.02.004.

[44] Liu, H., Chen, J., Chen, L., Xu, Y., Guo, X., Fang, D. (2016). Carbon Nanotube-Based Solid Sulfonic Acids as Catalysts for Production of Fatty Acid Methyl Ester via Transesterification and Esterification Carbon Nanotube-Based Solid Sulfonic Acids as Catalysts for Production of Fatty Acid Methyl Ester via Transesterif. *ACS Sustainable Chemistry & Engineering*, 4(6), 3140–3150. DOI: 10.1021/acssuschemeng.6b00156.

[45] Chang, C., Chang, K., Shen, H., Hu, C. (2014). A unique two-step Hummers method for fabricating low-defect graphene oxide nanoribbons through exfoliating multiwalled carbon nanotubes. *Journal of the Taiwan Institute of Chemical Engineers*, 45(5), 2762–2769. DOI: 10.1016/j.jtice.2014.05.030.

[46] Nda-umar, U.I., Irmawati, R., N. Muhamad, E., Azri, N., Ishak, N.S., Yahaya, M., Taufiq-Yap, Y.H. (2021). Journal of the Taiwan Institute of Chemical Engineers Organosulfonic acid-functionalized biomass-derived carbon as a catalyst for glycerol acetylation and optimization studies via response surface methodology. *Journal of Taiwan Institute of Chemical engineers*, 118, 355–370. DOI: 10.1016/j.jtice.2020.12.021.

[47] Pendolino, F., Armata, N. (2017). *Graphene Oxide in Environmental Remediation Process*. Springer Cham. DOI: 10.1007/978-3-319-60429-9

[48] Shen, Y., Yang, S., Zhou, P., Sun, Q., Wang, P., Wan, L., Li, J., Chen, L., Wang, X., Ding, S., Wei, D. (2013). Evolution of the band-gap and optical properties of graphene oxide with controllable reduction level. *Carbon*, 62, 157–164. DOI: 10.1016/j.carbon.2013.06.007.

[49] Li, Y., Liao, J., Wang, S., Chiang, W. (2016). Intercalation-assisted longitudinal unzipping of carbon nanotubes for green and scalable synthesis of graphene nanoribbons. *Nature Publishing Group*, 6(March), 1–12. DOI: 10.1038/srep22755.

[50] Mertsoy, E.Y., Sert, E., Atalay, S., Atalay, F.S. (2021). Fabrication of chromium based metal organic framework (MIL-101)/activated carbon composites for acetylation of glycerol. *Journal of the Taiwan Institute of Chemical Engineers*, 120, 93–105. DOI: 10.1016/j.jtice.2021.03.034.

[51] Dizoğlu, G., Sert, E. (2020). Fuel additive synthesis by acetylation of glycerol using activated carbon/UiO-66 composite materials. *Fuel*, 281, 118584. DOI: 10.1016/j.fuel.2020.118584.

[52] Fidelis Uchenna, A., Irmawati, R., Taufiq-Yap, Y.H., Mohd Izham, S., Nda-Umar, U.I. (2023). Glycerol acetylation over yttrium oxide (Y2O3) catalyst supported on palm kernel shell-derived carbon and parameters optimization studies using response surface methodology (RSM). *Arabian Journal of Chemistry*, 16(8), 104865. DOI: 10.1016/j.arabjc.2023.104865.

[53] Malaika, A., Mesjasz, D., Kozłowski, M. (2023). Maximizing the selectivity to triacetin in glycerol acetylation through a plastic waste-derived carbon catalyst development and selection of a reaction unit. *Fuel*, 333, 126271. DOI: 10.1016/j.fuel.2022.126271.